



Strategies for the quantification and characterization of nanoplastics in AOPs research

Carla di Luca^{a,b,**}, Jorge Garcia^a, Macarena Munoz^{a,*}, Mercedes Hernando-Pérez^{c,d,e}, Zahara M. de Pedro^a, Jose A. Casas^a

^a Departamento de Ingeniería Química, Universidad Autónoma de Madrid, Ciudad Universitaria de Cantoblanco, 28049, Madrid, Spain

^b División Catalizadores y Superficies, Instituto de Investigaciones en Ciencia y Tecnología de Materiales (INTEMA-CONICET), Av. Colón 10850, 7600, Mar del Plata, Argentina

^c Departamento de Física de los Materiales, Universidad Autónoma de Madrid, Ciudad Universitaria de Cantoblanco, 28049, Madrid, Spain

^d Instituto de Ciencia de Materiales Nicolás Cabrera, Universidad Autónoma de Madrid, Ciudad Universitaria de Cantoblanco, 28049, Madrid, Spain

^e Condensed Matter Physics Center (IFIMAC), Universidad Autónoma de Madrid, Ciudad Universitaria de Cantoblanco, 28049, Madrid, Spain

ARTICLE INFO

Keywords:

Nanoplastics
Characterization
Analysis
Polystyrene
Photo-Fenton
Advanced Oxidation Processes

ABSTRACT

There is a growing interest in developing new targeted degradation technologies for the removal of micro- and nanoplastics (NPs) in water, corresponding to increased public concerns regarding their potential negative impacts on urban water systems, and consequently on human life quality. Recently, Advanced Oxidation Processes (AOPs) have been proposed as promising treatment alternatives for effective degradation of NPs in water. However, the selection of appropriate analytical methods for monitoring these oxidation tests remains a challenge. Herein, the feasibility of different characterization strategies for monitoring the evolution of NPs in water upon oxidation tests was systematically studied using polystyrene (PS) NPs of different particle sizes ($D_0 = 140, 252, 460, \text{ and } 909 \text{ nm}$) as model plastic pollutants. To quantify NPs in water, Total Organic Carbon (TOC), Chemical Oxygen Demand (COD) and turbidity measurements were assessed. Moreover, turbidity was correlated to the particle size and PS NPs concentration by developing a response surface. Among the analytical techniques employed to characterize the solid particles, transmission electronic microscopy (TEM) was used to evaluate morphology and particle size. Alternatively, the viability of Dynamic Light Scattering (DLS), Nanoparticle Tracking Analysis (NTA) and Atomic Force Microscopy (AFM) to determine particle size is discussed. Chemical surface modifications were explored by Fourier-Transform Infrared Spectroscopy (FTIR). As a proof of concept, the degradation of PS NPs in water upon photo-Fenton oxidation was investigated at ambient conditions and fully characterized using the mentioned techniques.

1. Introduction

Polymers are among the most important materials families of the 21st century, with their ubiquitous use strongly shaping various aspects of our daily lives. Accordingly, global plastic production reached nearly 400 million tons in 2022 [1], and it is projected to double over the next two decades [2]. Depending on their application, plastic products can have lifespans ranging from just a single day to well beyond 50 years before becoming plastic waste. Unfortunately, up to 71 % of it end up in the environment [3]. Once in the environment, plastic debris undergoes a series of transformations, including fragmentation into smaller pieces.

Particles smaller than 5 mm are classified as microplastics (MPs), while those below 1 μm are defined as nanoplastics (NPs) [3]. Due to their tiny size, NPs are regarded as potentially the most harmful, exhibiting distinct physicochemical features than MPs [4].

Nowadays, plastic debris have been detected across diverse environmental matrices, including water, air, soil, sediment, and living organisms. Notably, plastic waste in urban water systems has become a growing concern due to its potential impact on human life quality [4,5]. Recent studies have identified municipal wastewater treatment plants (WWTPs) as hotspots of this type of pollution [6,7]. While WWTPs can achieve removal efficiencies exceeding 90 % for MPs, they remain the

* Corresponding author.

** Corresponding author at: Departamento de Ingeniería Química, Universidad Autónoma de Madrid, Ciudad Universitaria de Cantoblanco, 28049, Madrid, Spain.
E-mail addresses: cardiluca@fi.mdp.edu.ar (C. di Luca), macarena.munnoz@uam.es (M. Munoz).

<https://doi.org/10.1016/j.cej.2024.152490>

Received 21 March 2024; Received in revised form 7 May 2024; Accepted 22 May 2024

Available online 22 May 2024

1385-8947/© 2024 The Authors. Published by Elsevier B.V. This is an open access article under the CC BY-NC-ND license (<http://creativecommons.org/licenses/by-nc-nd/4.0/>).

primary source of these particles in aquatic environments, largely due to the huge volume continuously discharged by these facilities. In this context, the development of innovative and sustainable water treatment technologies has been encouraged among the scientific community to prevent the release of MPs and NPs from WWTPs [8–10].

Recent research has stated that advanced oxidation processes (AOPs) hold great potential as tertiary treatments for the degradation of MPs and NPs in aqueous systems [8,11–13]. These processes involve the *in-situ* generation of non-selective oxidative radicals, enabling the breakdown of complex organic compounds into less/non-hazardous small molecular compounds [14]. Among the most representative studies, TiO_2 structures were employed for the photocatalytic oxidation of PS NPs at room temperature, resulting in a mineralization rate of up to 13 % after 50 h reaction time [15]. Two other photo-assisted methods, such as UV/peroxymonosulfate and UV/ H_2O_2 , have been recently explored for the degradation of PS NPs and PET microfibers, respectively, achieving notable levels of mineralization (c.a. 64 % for PS NPs) and mass losses (up to 21.6 % for PET fibers) [16,17]. Li et al. observed 99.9 % molecular weight degradation of PS NPs and 42.7 % mineralization in 240 min of single ozonation [18]. In a subsequent study, the use of a CeOx@MnOx catalyst significantly enhanced the efficacy of single ozonation, leading to 96.7 % reduction in molecular weight of PS NPs within 50 min reaction time [19]. In our recent contributions, up to 70 % mineralization of PS NPs was achieved by Fenton oxidation after 7.5 h reaction time at 80 °C, by using sequential reagents dosages [20]. However, by intensifying the process using a broad-spectrum UV–Vis lamp, complete mineralization of PS NPs was yielded within 40 min reaction time under ambient conditions [12]. Besides these initial contributions, it is worth noting that the study of these treatment technologies is still in its early stages, and further research is required to enhance the efficiency of the proposed processes. Likewise, NPs degradation has received considerably less attention than MPs, mainly due to the complexity of the analytical methods needed and the difficulty of obtaining representative model NPs or realistic samples [21].

Regarding NPs characterization, there are still significant challenges to overcome. These challenges stem from the limited sensitivity of mass-based analytical tools, needing a preconcentration step due to the low concentration of NPs solutions, and the small size of the particles, which falls below the optical resolution, requiring more complex techniques and equipment [4,22]. Before evaluating the efficiency of the applied treatment, it is crucial to establish efficient and accurate methods for identifying and quantifying NPs in water [11]. Usually, the colloidal nature and dominant Brownian motion of NPs hinder their sedimentation, compared to MPs made from the same material. To evaluate the progress of an oxidative degradation, it is essential to employ a combination of quantification and identification techniques. Among the available analytical methods, Total Organic Carbon (TOC), Turbidity and Gel Permeation Chromatography (GPC) were among the most used techniques for monitoring the oxidation advance [12,15,17–19,23]. Fourier-transform infrared spectroscopy (FTIR) was employed not only to identify polymer types but also to evaluate post-treatment chemical alterations, such as the incorporation of oxygenated groups [15,18,20,23–25]. Likewise, X-ray photoelectron spectroscopy (XPS) was employed to evaluate the chemical states of carbon and oxygen atoms before and after the treatment [25]. Even though polymers show poor contrast in transmission electron microscopy (TEM), this technique has been employed to determine particle size and shape of NPs suspensions [12,16,18,25]. Alternatively, microscopy techniques can be employed to evaluate the reduction of particle volume and estimate the degree of conversion [26]. To elucidate the oxidation mechanism, gas chromatography-mass spectrometry (GC–MS) was the most frequently employed technique [15,18,23,27].

The aim of this work was to investigate the application of different characterization techniques for monitoring the degradation of nanoplastics (NPs) in water upon advanced oxidation processes. For such goal, polystyrene nanoplastics (PS NPs) of different particle size (140 –

909 nm) were used as model plastic pollutants, and their oxidation upon photo-Fenton treatment was fully characterized. The mineralization of PS NPs was assessed by TOC and COD, and its concentration by turbidity measurements. PS nanoparticle size was determined using TEM, dynamic light scattering (DLS), nanoparticle tracking analysis (NTA) and atomic force microscopy (AFM), discussing the limitations of each technique. Moreover, a correlation between turbidity, particle size and PS NPs concentration was developed as a rapid tool to assess the evolution of the concentration from turbidity and particle size measurements. The chemical composition of fresh and oxidized NPs samples was examined by FTIR, and the carbonyl index was calculated as an indicator to measure the oxidation degree in PS NPs.

2. Materials and methods

2.1. Materials and chemicals

Four commercial samples of monodisperse polystyrene nanospheres, PS-R-KM248 ($D_0 = 140 \pm 5$ nm, 5 % w/v), PS-R-KM239 ($D_0 = 252 \pm 6$ nm, 5 % w/v), PS-R-KM378 ($D_0 = 460 \pm 10$ nm, 5 % w/v), and PS-R-KM123 ($D_0 = 909 \pm 27$ nm, 5 % w/v), were purchased from micro-Particles GmbH and labelled here as PS140, PS252, PS460 and PS909, respectively. Nitric acid (65 %), titanium (IV) oxysulfate (99 %), potassium dichromate (>99 %), sulfuric acid (98 %), ferrous ammonium sulfate (>99 %), ferrous sulfate heptahydrate (>99 %), 1,10-phenanthroline monohydrate (>99 %), and iron (III) nitrate nonahydrate (98 %) were provided by Sigma-Aldrich. Silver sulfate (>99 %) was provided by Fluka. Hydrogen peroxide solution (33 % w/w) was supplied by Panreac. All these compounds were used as received without further purification. Deionized water was used as reaction matrix to perform the photo-Fenton experiments. Alternatively, a secondary wastewater treatment plant effluent from the Autonomous University of Madrid (pH = 7.04; Conductivity = $615 \mu\text{S cm}^{-1}$; $\text{Cl}^- = 196.53 \text{ mg L}^{-1}$; $\text{SO}_4^{2-} = 16.77 \text{ mg L}^{-1}$; $\text{NO}_3^- = 64.68 \text{ mg L}^{-1}$; Turbidity = 2.44 NTU; Total Carbon = 10.65 mg L^{-1} ; TOC = 6.337 mg L^{-1} ; Inorganic Carbon = 4.309 mg L^{-1}) was used as water matrix in a photo-Fenton test.

2.2. Analytical methods

On the one hand, the mineralization of PS NPs ($D_0 = 140$) was determined by the analysis of Total Organic Carbon (TOC) using a TOC analyzer (Shimadzu TOC VSCH). It must be noted that the PS NPs tested in this work remained in a stable suspension in water regardless of their particle size. On the other hand, PS NPs mineralization was also quantified by Chemical Oxygen Demand (COD) measurements by using the standard open reflux method [28]. Since the presence of hydrogen peroxide interferes with COD measurements, its residual concentration was eliminated by employing a Pt catalyst (50 g/L, 120 min at room temperature) previous to the COD measurements. Hydrogen peroxide was determined by colorimetry using a Varian Cary 5000 UV–Visible Spectrophotometer, following the titanium oxysulfate method [29]. Turbidity was determined with a benchtop turbidity meter HI88713 (Hanna Instruments). Turbidity, particle size and NPs concentration were correlated by developing a response surface. For this purpose, experimental calibration curves of turbidity were determined in the range 0 – 100 mg/L and for different nominal diameters of PS NPs. Subsequently, the experimental data were fitted to a response surface using a second-degree polynomial model, adjusted by the Least-Squares regression method in Python. All calibration curves reported in this work were performed in triplicate with standard deviation < 5 %, represented as the error bars in the reported figures.

The particle size of the PS NPs was determined by Transmission Electron Microscopy (TEM) using a JEOL JEM 2100 microscope with a 0.25 nm point resolution. A few drops of PS NPs suspensions were manually deposited on Formvar Carbon coated 200 mesh copper grids. The software “ImageJ” was used for measuring and counting the NPs

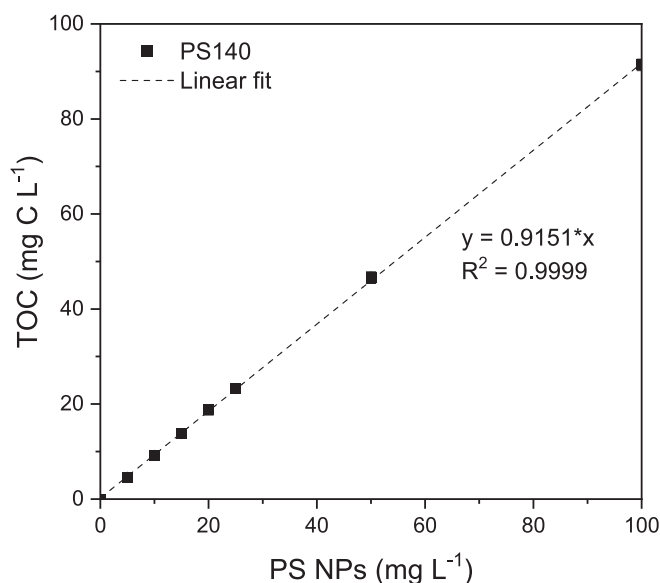


Fig. 1. Calibration curve of Total Organic Carbon (TOC) vs. PS NPs concentration ([PS NPs] = 0 – 100 mg/L and $D_0 = 140$ nm).

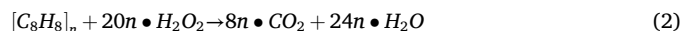
spheres (more than 200 particles per sample were considered when possible). Alternatively, multiangle Dynamic Light Scattering (DLS) was conducted using the Zetasizer Ultra (Malvern Panalytical, UK). Typical sample volumes of approximately 1 mL were loaded into a DTS0012 cuvette, with Nonidet P 40 serving as the dispersant. Each sample was measured by triplicate at three different angles to account for front (13), side (90) and back (173) scatter of light. Data processing was carried out using the ZS Xplorer Software Suite v3.1.0.64. The calculations used a refractive index of 1.59 and absorption of 0.01. Also, particle size distribution of PS NPs was carried out by Nanoparticle Tracking Analysis (NTA) with a NanoSight NS300 (Malvern Panalytical) equipped with a 488 nm laser module. The camera operated at 25 frames per second, capturing a video file of the particles moving under Brownian motion. Each sample was recorded three-fold. The software tracked many particles individually and using the Stokes-Einstein equation calculated their hydrodynamic diameters. A home-built Atomic Force Microscope (AFM) operating in dynamic mode was employed to measure the diameter of the PS NPs. Functionalized mica with 5 % APTS in Milli-Q water ((3-aminopropyl) triethoxysilane, Sigma Aldrich) was used as a substrate for the PS NPs. Subsequently, a 30 μ L droplet of the sample was incubated for 45 min at 20 °C. Following incubation, the samples underwent a single rinse with Milli-Q water and subsequently dried. AFM measurements were performed by using PPP-FR NANOSensors rectangular cantilevers ($L = 225$ μ m, $W = 28$ μ m), with a nominal spring constant of 2.8 N/m and a tip radius of c.a. 10 nm. Subsequently, height profiles were generated, analyzed, and processed using WSxM 5.0 software [30].

The surface chemistry of fresh and oxidized PS NPs was evaluated by Fourier-Transform Infrared Spectroscopy (FTIR) using a Spectrum Two FTIR spectrometer by Perkin Elmer. The analyses were carried out by the attenuated total reflectance (ATR) method using a diamond crystal. The resolution used was 4 cm^{-1} , an aperture of 8.94 mm, and 20 scans were recorded for each sample. The carbonyl index (CI) was calculated by means of the procedures reported in the literature [13,31]. In brief, CI was calculated as the ratio of the maximum absorbance height of the carbonyl group (A_C) around 1716 cm^{-1} relative to the maximum absorbance height of a reference peak (A_{Rp}) at 2850 cm^{-1} according to Eq. (1).

$$CI = A_C/A_{Rp} \quad (1)$$

2.3. Photo-Fenton oxidation procedure

The experimental setup used was similar to the one described in a prior publication [12]. Briefly, photo-Fenton experiments were performed in an immersion-wall batch jacketed photoreactor (0.7 L) equipped with a 150 W medium pressure Hg lamp (Nova Light TQ-150 from Pechl Ultraviolet) confined in a water-cooled quartz chamber provided with a temperature control unit (Ministat 125, Huber). The lamp emits in a broad-spectrum between 250 and 600 nm with a UV-irradiance of 200 W m^{-2} . The case study was carried out under optimized operation conditions: $[\text{PS NPs}]_0 = 100 \text{ mg L}^{-1}$, $D_0 = 140, 252, 460$ and 909 nm, $[\text{H}_2\text{O}_2]_0 = 1000 \text{ mg L}^{-1}$, $[\text{Fe}^{3+}]_0 = 1 \text{ mg L}^{-1}$, $\text{pH}_0 = 3$ and $T = 25$ °C. About the hydrogen peroxide dosing strategy, additional doses ($[\text{H}_2\text{O}_2] = 500 \text{ mg L}^{-1}$) were added to the reactor every 30 min to enhance the oxidation yield. The complete PS NPs mineralization proceeds according to Eq. (2). The reaction experiments were performed in triplicate with standard deviation < 10 %, depicted as the error bars in the reported figures.



The conversion of PS nanospheres ($X_{\text{PS NPs}}$) can be calculated from particle size analysis (X_{TEMi}) based on the geometry of spherical particles (Eq. (3)), where r_i represents the radius of individual particles measured by TEM at a certain reaction time, and r_0 is the initial particle radius. As the degradation proceeds, the oxidized NPs increase the breadth of the particle size distribution, resulting in a PS NPs conversion distribution. Thus, PS NPs conversion was determined as the weighted average value (X_{TEM}), considering the volume of individual particles V_i and their total volume V (Eq. (4)). As well, the conversion of PS NPs was determined from turbidity measurements (X_{Turbid}) (Eq. (5)) and contrasted with the values obtained from particle size analysis.

$$X_{\text{TEMi}} = 1 - (r_i(t)/r_0)^3 \quad (3)$$

$$X_{\text{TEM}} = \sum X_{\text{TEMi}} \bullet \frac{V_i}{V} \quad (4)$$

$$X_{\text{Turbid}} = 1 - (\text{Turbidity}(t)/\text{Turbidity}_0) \quad (5)$$

3. Results and discussion

3.1. Quantification of PS NPs in water

3.1.1. Total Organic Carbon (TOC)

TOC is an analytical parameter that indicates the total amount of organic carbon in dissolved or suspended compounds present in aqueous samples. Nanoplastics can be classified as forms of non-dissolved organic matter. However, as their degradation in water advances, they may release dissolved organic carbon as partial oxidation by-products [32,33]. TOC analysis is inherently destructive, and the combustion catalytic oxidation method employed, typically carried out at 680 °C, achieves total combustion of hard-to-decompose organic compounds, including insoluble and macromolecular organic compounds. Moreover, TOC analysis provides a bulk parameter as it is representative of the entire suspension. Based on the molecular formula of PS, the theoretical carbon concentration of 20 mg L^{-1} PS NPs corresponds to 18.46 mg C L^{-1} , which clearly matches with the experimental calibration curve displayed in Fig. 1 (Slope = 0.9151 $\text{mg C mg PS NPs}^{-1}$ and $R^2 = 0.9999$). It is important to highlight that TOC values are independent of the NPs particle size and nature and depend solely on the content of carbon present in the sample being analyzed [31]. According to the manufacturer, colloidal suspensions of NPs can be accurately measured by TOC. However, it should be noted that larger NPs, such as those with a particle diameter close to 1000 nm, can cause maintenance issues in the equipment due to particle accumulation in the piping and sampling/injection systems. Consequently, TOC measurements are recommended

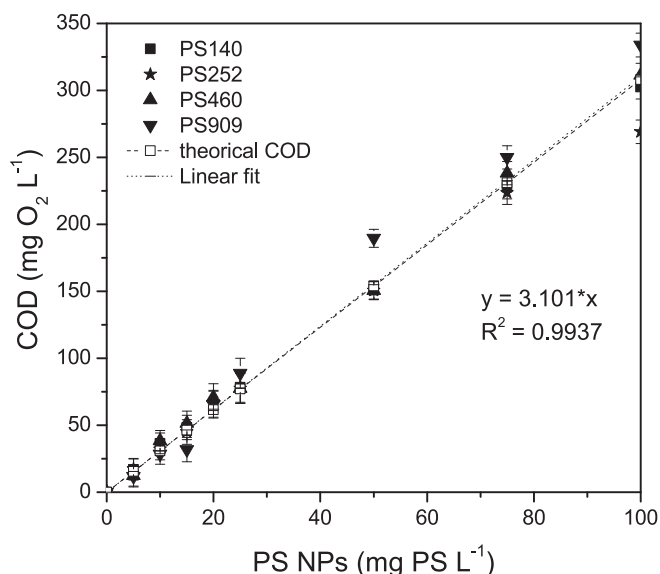


Fig. 2. Calibration curve of Chemical Oxygen Demand (COD) vs. PS NPs concentration ([PS NPs] = 0 – 100 mg/L and D_0 = 140, 252, 460 and 909 nm).

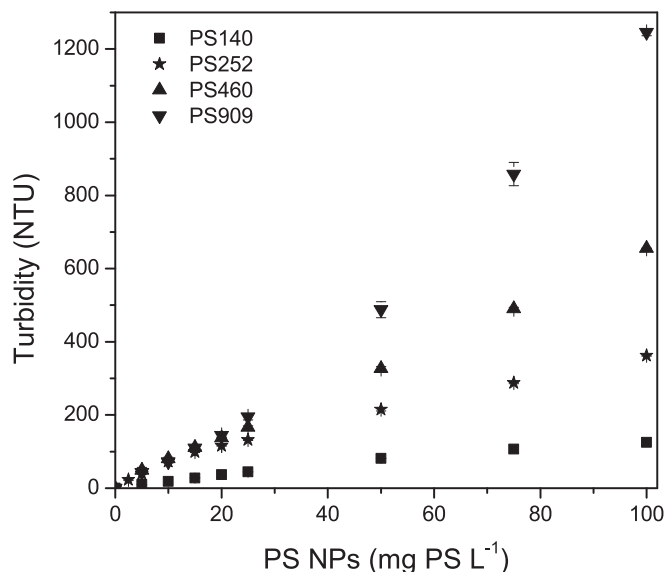


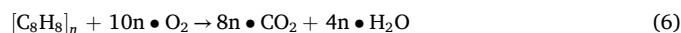
Fig. 3. Calibration curves of turbidity vs. PS NPs concentration ([PS NPs] = 0 – 100 mg/L and D_0 = 140, 252, 460 and 909 nm).

for determining the NPs concentration in dilute samples of small particles (c.a. 100 nm) and/or in advanced stages of the oxidative treatment under study.

3.1.2. Chemical Oxygen Demand (COD)

In environmental chemistry, COD is an indicative measure of the amount of oxygen required to chemically oxidize the organic matter and inorganic compounds present in water, under controlled conditions. The COD analysis is also a destructive method that involves the digestion of dissolved and insoluble compounds in a boiling mixture of a known excess of potassium dichromate in sulfuric acid reagent using Ag_2SO_4 as catalyst. After digestion at 150 °C, the remaining unreduced $\text{K}_2\text{Cr}_2\text{O}_7$ is titrated to determine the amount consumed, allowing for the calculation of the oxidizable matter in terms of oxygen equivalent with units of $\text{mg O}_2 \text{ L}^{-1}$ [28]. It is important to consider potential interferences from halides and contributions from reduced inorganic species when performing

this analysis. So far, COD analysis has been employed to evaluate the formation of dissolved by-products during the photo-oxidation of PET and PA66 microfibers (MFs) [16,34]. However, these studies focused only on the amount of COD present in the leachates, separating the MFs from the reaction supernatant. To the best of our knowledge, COD measurements have not yet been reported for assessing mineralization levels by digesting the plastic particles themselves. Fig. 2 shows the calibration curves of COD for different concentrations and particle sizes of PS NPs. The linear fitting of all the experimental data compiled in the range under study displayed a slope of $3.101 \text{ mg O}_2 \text{ mg PS NPs}^{-1}$ and an $R^2 = 0.9937$. According to Eq. (6), the stoichiometric amount of oxygen required for complete oxidation of PS is $3.08 \text{ g O}_2 \text{ g PS}^{-1}$, or equivalently, $3.30 \text{ g O}_2 \text{ g C}^{-1}$. These values align quite well with the calibration curves depicted in Fig. 2. This confirms that the solid nanoparticles were completely digested using the standard open reflux method, validating COD measurements as an accurate technique for monitoring NPs mineralization. Again, it is important to note that COD values are independent of the particle size and nature of NPs and depend exclusively on the content of oxidizable matter in the sample. As well, this technique provides a bulk parameter.



3.1.3. Turbidity

Turbidity in water is caused by suspended and colloidal matter. This parameter reflects the optical properties that causes light to be scattered and absorbed rather than transmitted with no change in direction or flux level through the sample. The size, shape, and refractive index of the particles generally influence the light-scattering properties of the suspension [28]. Fig. 3 displays the calibration curves of different concentrations and particle sizes of PS nanospheres. Contrary to the results obtained with TOC and COD measurements, it can be clearly observed that turbidity depends on both the particle size and NPs concentration. Additionally, this technique is non-destructive, allowing for liquid samples to be returned to the reactor after analysis, and offers a bulk measurement. Nevertheless, the simultaneous presence of other light-absorbing substances, such as iron precipitates, colored dissolved organic matter or powdered photocatalysts, may cause a negative interference in the measurements.

Fig. 4 and Fig. 5 depict a correlation between the calibration curves displayed in Fig. 3. It can be observed that second-degree polynomial models fit well the concentration range under study. According to the trends of the parameters being related, it is necessary to split the adjustment into two concentration ranges (Eqs. (7) and (8)), where [PS NPs] represents the concentration of PS NPs, and D_p represents the particle diameter. Similarly, the values of COD or TOC could be easily related to turbidity values through the calibration curves displayed in Figs. 1 and 2. Nevertheless, for a more in-depth analysis, it should be considered that dissolved organic carbon may be present in the reaction medium due to the leaching of oxidation intermediates. While it may not directly contribute to turbidity measurements, it can still affect the degree of mineralization achieved.

For [PS NPs] = 0 – 20 mg L^{-1} :

$$\text{Turbidity} = -0.00032 \bullet D_p^2 - 0.086 \bullet [\text{PSNPs}]^2 + 0.0049 \bullet D_p \bullet [\text{PSNPs}] + 0.34 \bullet D_p + 5 \bullet [\text{PSNPs}] - 58 \quad (R^2 = 0.9559) \quad (7)$$

For [PS NPs] = 20 – 100 mg L^{-1} :

$$\text{Turbidity} = -0.00081 \bullet D_p^2 + 0.012 \bullet [\text{PSNPs}]^2 + 0.018 \bullet D_p \bullet [\text{PSNPs}] + 0.47 \bullet D_p - 2.8 \bullet [\text{PSNPs}] + 10 \quad (R^2 = 0.9980) \quad (8)$$

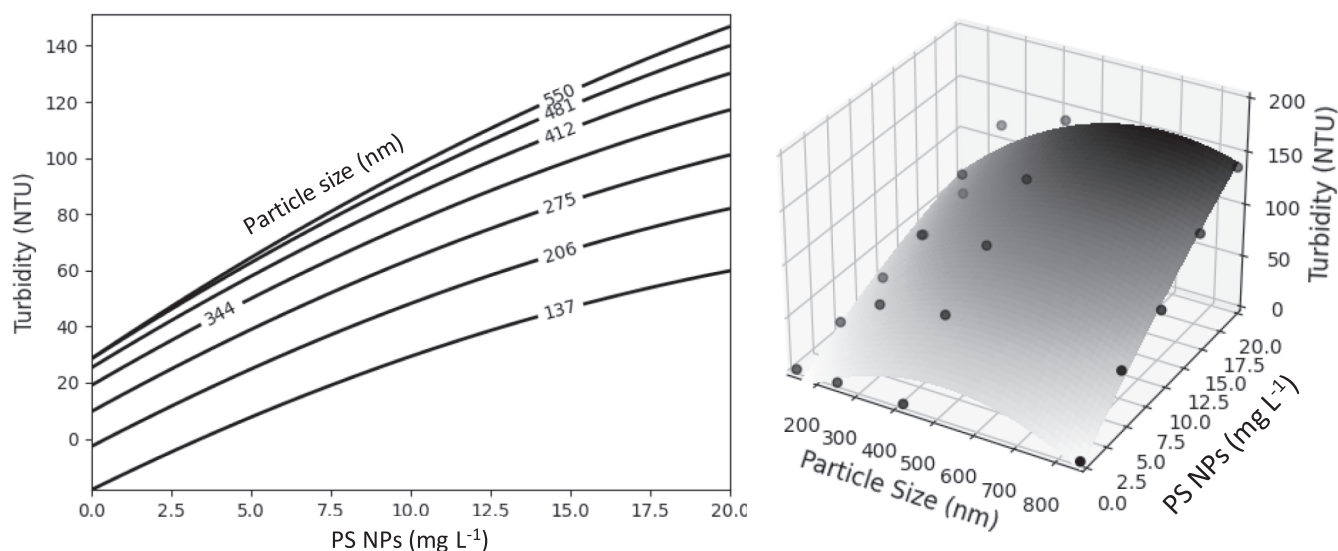


Fig. 4. Correlation between turbidity, PS NPs concentration and particle size in the low range of concentration ([PS NPs] = 0 – 20 mg/L).

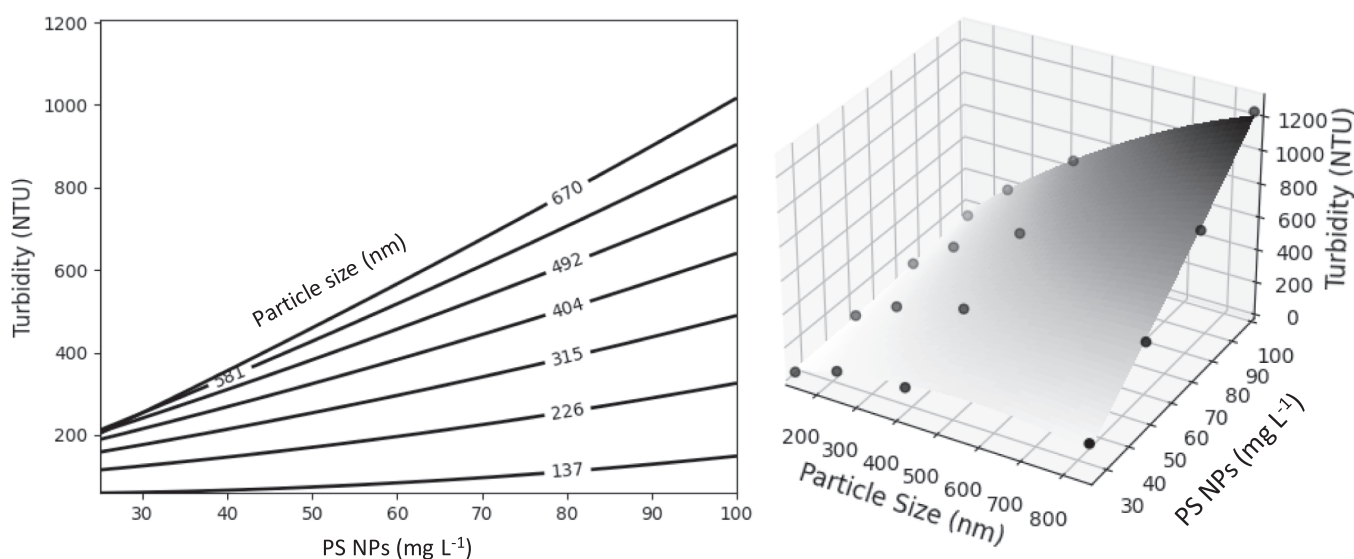


Fig. 5. Correlation between turbidity, PS NPs concentration and particle size in the high range of concentration ([PS NPs] = 20 – 100 mg/L).

3.2. Assessment of NPs particle size

3.2.1. Transmission Electronic Microscopy (TEM)

TEM stands as the predominant method for characterizing nanomaterials, providing micrographs at a spatial resolution equal to the level of atomic dimensions. In general, polymers are composed of elements that show poor contrast in TEM because their elastic interactions with electrons are weak [35]. Nevertheless, for NPs with defined morphology and samples suspended in a clean water matrix, it has shown to be an excellent technique to evaluate the particle size. Fig. 6 displays the TEM micrographs of PS NPs, confirming their sphericity and monodispersity. From the particle size analysis, it should be noted that the fresh samples exhibited slightly smaller diameters than those reported by the manufacturer (Table 1). Moreover, it is important to note that an accurate determination of both mean diameter and particle size distribution requires a thorough count of particles, which can be time consuming.

3.2.2. Dynamic Light Scattering (DLS)

DLS employs a laser beam to pass through a liquid suspension of

analyte particles, which scatter the incident laser at different scattering angles. The Brownian motion of these particles induces a shift in light frequency, which varies with different particle sizes. Consequently, the hydrodynamic diameter and size distribution of the measured particles can be calculated by analyzing the scattered light signal over time in conjunction with the Stokes-Einstein equation [36]. This technique is non-invasive and allows for the analysis of low sample volumes. In this system, suspended particles scatter incident light with signal intensity proportional to the sixth power of particle radii [37]. Therefore, larger particles scatter much more intensely than smaller ones. This can lead to the signals from larger particles overshadowing those of smaller particles, potentially causing smaller particles to be overlooked in the analysis of a polydisperse sample [36,38]. Accordingly, Table 1 shows that DLS results gave mean diameters somewhat higher (c.a. 9 – 21 %) than those obtained by TEM analysis. Hence, owing to the intrinsic limitations of DLS, this technique may not be suitable for analyzing oxidized samples with a broader particle size distribution and/or particle agglomerates.

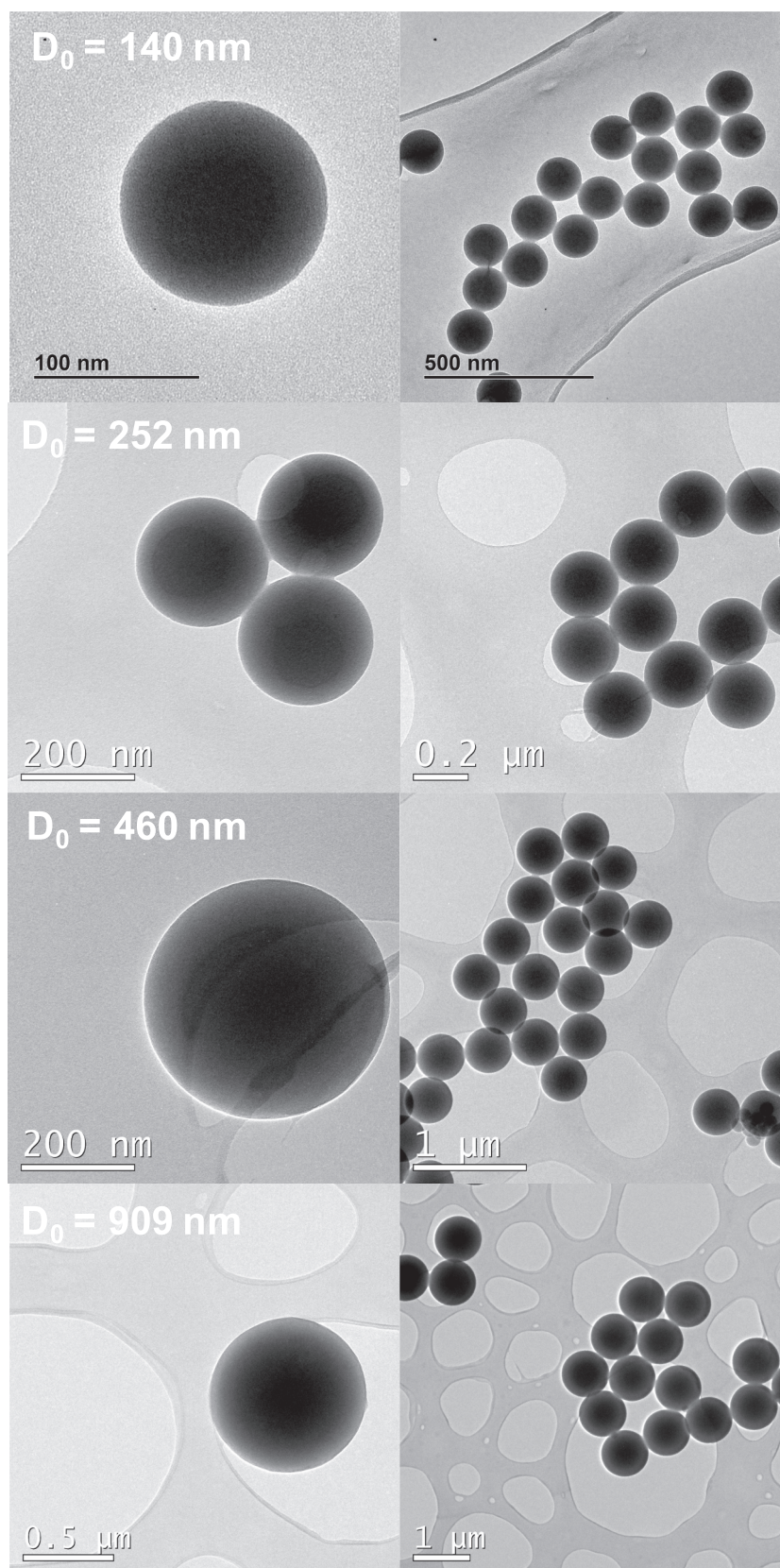


Fig. 6. TEM analysis of PS NPs with different particle sizes.

Table 1

Comparison of particle size analysis of fresh PS NPs samples using TEM, DLS, NTA and AFM.

Nominal diameter (nm)	TEM	DLS	NTA	AFM
140	137.4	149.7	135.9	137.7
252	247.5	278.3	229.5	247.0
460	440.5	505.4	345.6	---
909	873.1	1033	723.5	---

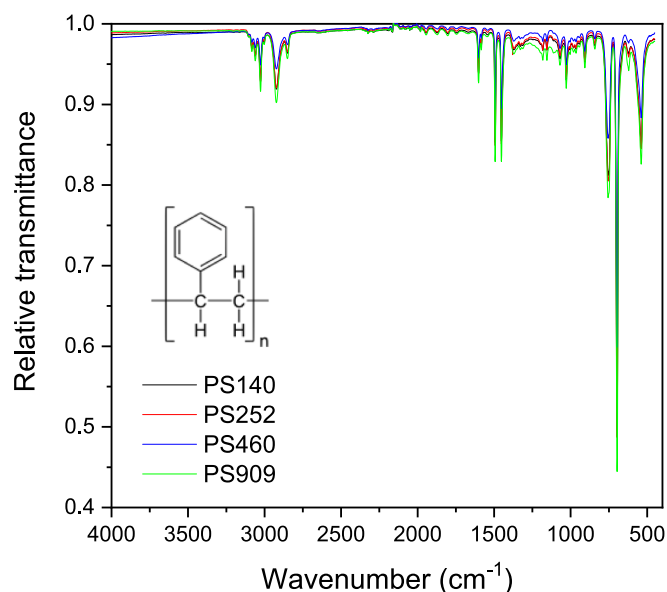


Fig. 7. FTIR spectra of PS NPs with different particle sizes (140, 252, 460 and 909 nm).

3.2.3. Nanoparticle Tracking Analysis (NTA)

Based on similar principles to DLS, NTA employs intense laser light to illuminate particles in suspension, tracking individual particles and recording their motion frame by frame using a high-sensitivity camera. However, the accuracy of NTA is restricted by the limitations of Brownian motion, wherein particles move randomly at a speed proportional to their size, with larger particles exhibiting slower motion than smaller particles [36]. From Table 1, particles smaller than 300 nm exhibited mean diameters similar to those obtained by TEM (c.a. 1 – 7 %). However, larger particles displayed higher deviations in the mean diameter (c.a. 15 – 21 %), probably due to the limitations of Brownian motion. Consequently, NTA can be suitable for tracking smaller particles. However, it is important to note that oxidized samples may form aggregates and may become too diluted for NTA. Therefore, proper sample preparation may require the preconcentration of samples, along with the use of an appropriate dispersant and sonication.

3.2.4. Atomic Force Microscopy (AFM)

AFM is a fundamental tool in the field of nanotechnology, particularly for characterizing the height of nanoparticles and their surface morphology [39]. Unlike SEM, AFM allows measurements on non-conductive materials without the need for surface metallization. In the sample preparation for SEM analysis, to enhance conductivity, coatings applied to polymers can lead to misclassification of MPs and NPs or induce morphology changes [40]. AFM operates by scanning the surface of samples with a tiny rigid tip. When the tip is in the close proximity of the sample surface, it experiences interaction forces that produce the deflection of a cantilever and, when the cantilever is oscillating, alterations in magnitudes related to the dynamics of the cantilever. Either the deflection (contact mode) or a magnitude of its dynamics (e.g.

amplitude, frequency, phase or dissipation) serves as feedback signal. The feedback system then adjusts the distance between the tip and the sample by moving the piezoelectric Z to ensure that the feedback signal remains constant. The resulting changes in distance produce a surface topography image. AFM offers several advantages, including high-resolution nanoscale imaging, preservation of the sample surface (non-destructiveness), applicability to non-conductive polymers, and the generation of direct 3D surface images [35].

AFM measurements of fresh PS NPs (140 nm and 252 nm) yielded a mean diameter of 137.7 nm and 247.0, respectively, aligning closely with TEM results (Table 1 and Fig. S1) and thus establishing AFM as a reliable technique for assessing the particle size of NPs.

3.3. Evaluation of NPs chemical composition

3.3.1. Fourier-Transform Infrared Spectroscopy (FTIR)

Infrared spectroscopy is an absorption spectroscopic technique generally used for the study of chemical bonds in the field of materials characterization. When an infrared photon is absorbed by a molecule, it passes from its fundamental vibrational state to an excited vibrational state. The vibrations can be of two types: stretching of the chemical bond and deformation of the bond angle (bending) [35]. Some of the advantages of this technique include non-destructiveness, low sample requirements, representativeness of sample bulk, and environmental friendliness [41]. Together with Raman spectroscopy, FTIR is an outstanding technique to characterize the nature of polymers.

Fig. 7 displays the FTIR spectra of the fresh PS NPs under study. For this polymer, the absorption peaks at 756 and 698 cm^{-1} correspond to C-H out-of-plane bending vibration absorption indicating that the benzene ring has only one substituent. Also, PS displays absorption peaks between 1620 and 1400 cm^{-1} due to aromatic C = C stretching vibration of aromatic rings. This polymer has only two saturated C-H stretching peaks between at 2923 and 2850 cm^{-1} , related to methyl groups. Also, the unsaturated C-H stretching peaks appear at 3081, 3059, and 3025 cm^{-1} [42].

3.4. Characterization of the evolution of NPs degradation in water: A case study for the photo-Fenton oxidation of PS NPs

Fig. 8 displays the performance of the photo-Fenton treatment applied to PS NPs with different particle sizes, under optimized operating conditions: $[\text{PS NPs}]_0 = 100 \text{ mg L}^{-1}$; $[\text{Fe}^{3+}]_0 = 1 \text{ mg L}^{-1}$; $[\text{H}_2\text{O}_2]_0 = 1000 \text{ mg L}^{-1}$ (H_2O_2 dosed every 30 min, 500 mg L^{-1}); $\text{pH}_0 = 3$ and $T = 25^\circ\text{C}$. In these tests, the oxidation progress was monitored in terms of turbidity, H_2O_2 concentration, COD, TEM, and TOC (when possible). Additionally, the particle size of selected oxidized samples was also measured by DLS and AFM, and the surface chemistry modifications were analyzed by FTIR. From Fig. 8a, it can be observed that the turbidity of the reaction medium decreased from its initial value until reaching a completely clear solution within 75 – 90 min reaction time (see the inserts at Fig. 8b), achieving complete conversion of PS NPs (Fig. 8c). Clearly, the photo-Fenton process, using broad-spectrum UV-irradiance ranging from 250 to 600 nm as the light source, exhibits outstanding performance at ambient conditions and can be applied to PS NPs of different particle sizes, demonstrating its feasibility across a broad range of particle size. Accordingly, when larger PS particles are being treated, the PS NPs removal rate slows down slightly, likely due to both a reduced surface to volume ratio and a lower irradiance reaching the NPs surface (since larger particles give rise to higher turbidity values as shown in Fig. 3). Due to the irradiation source employed, hydrogen peroxide degrades quickly (blue lines and markers in Fig. 8a). Hence, to enhance mineralization yield further, a strategy of multiple-step H_2O_2 addition was adopted (see Materials and Methods Section).

In this process, the kinetic rate and oxidation yield is a combination of direct photolysis, the photolysis of hydrogen peroxide molecule, the photosensibilization of aquated ferrous/ferric complexes and Fenton

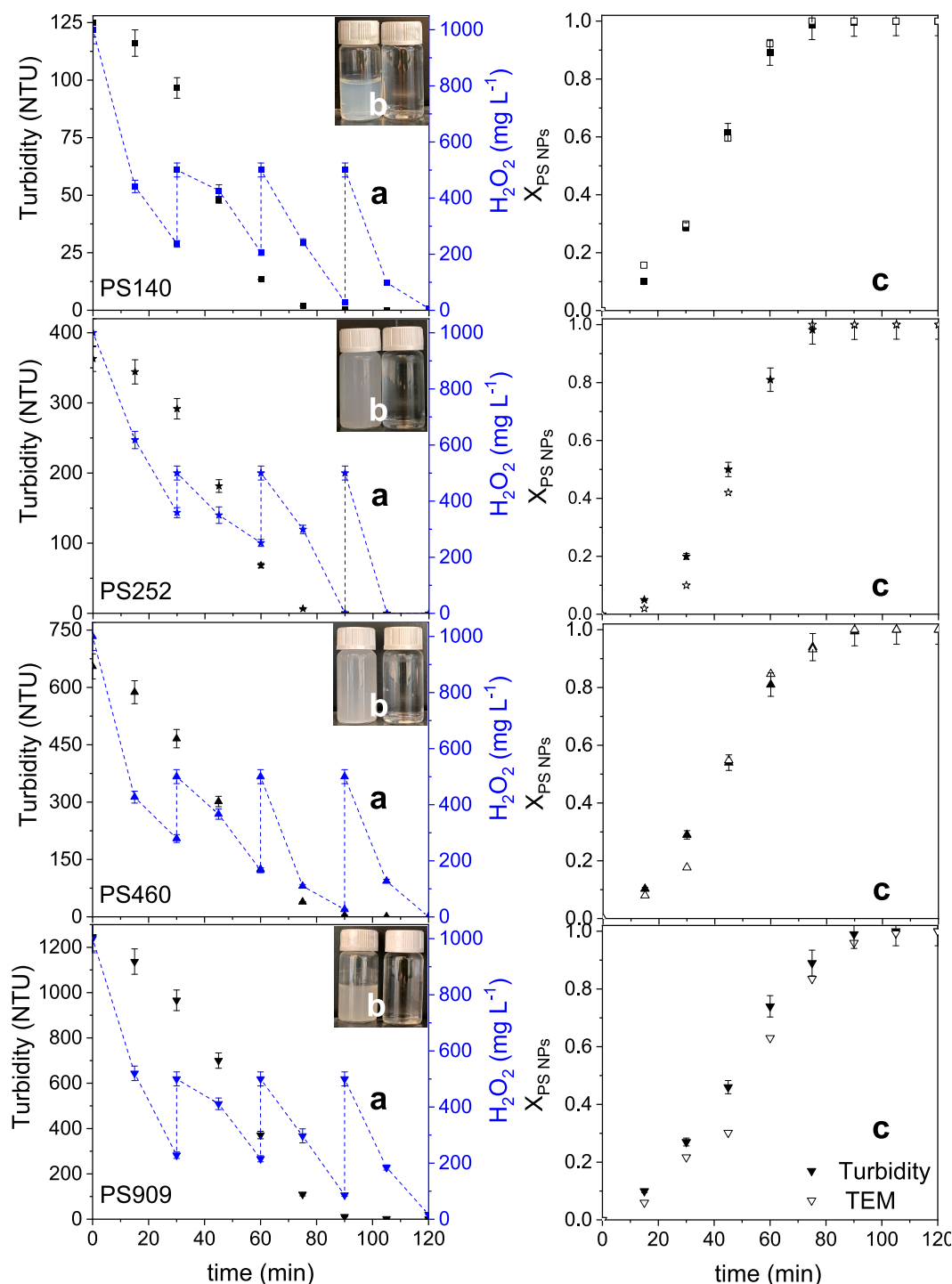


Fig. 8. Photo-Fenton oxidation of PS NPs of different particle sizes: a) turbidity and hydrogen peroxide evolution, b) Visual inspection of the reaction volume without treatment and at final reaction time, and c) PS NPs conversion determined from turbidity (black markers) and TEM (white markers) measurements ($D_0 = 140, 252, 460$ and 909 nm; $[PS\ NPs]_0 = 100$ mg/L; $[Fe^{3+}]_0 = 1$ mg/L; $[H_2O_2]_0 = 1000$ mg/L (H_2O_2 dosed every 30 min, 500 mg/L); $pH_0 = 3$; $T = 25$ °C).

reactions, thus intensifying the production of hydroxyl radicals [12]. According to the literature, the reaction is initiated by the attack of $HO\bullet$ radicals on the surface of PS NPs. This attack generates carbon-centered radicals within the polymer structure. Subsequently, these radicals can react with dissolved oxygen, leading to the formation of peroxide molecules. The third step possibly involves the production of hydroperoxide compounds when peroxide interacts with water molecules. Further reactions can result in chain scission and the formation of carbonyl or ketone compounds. These oxidation intermediates can then undergo

further degradation into short-chain acids and ultimately decomposed to CO_2 and water (mineralization). It is important to note that UV photons can directly be absorbed by the polymeric chains, creating excited states that generate chain scission, cross-linking, and polymer oxidation [31,43].

Under the studied conditions, a remarkable level of mineralization ($>80\%$ TOC removal and 95% COD removal) of PS NPs (140 nm) was achieved within 90 min reaction time (Fig. 9). The outstanding performance of the photo-Fenton process can be attributed to the wavelength

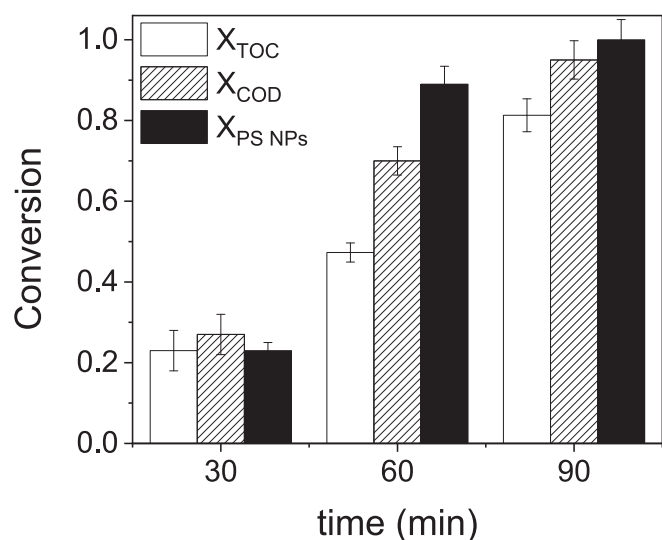


Fig. 9. Conversion of TOC, COD, and PS NPs upon photo-Fenton oxidation of PS NPs ($D_0 = 140$ nm; $[PS\ NPs]_0 = 100$ mg/L; $[Fe^{3+}]_0 = 1$ mg/L; $[H_2O_2]_0 = 1000$ mg/L (H_2O_2 dosed every 30 min, 500 mg/L); $pH_0 = 3$; $T = 25$ °C).

range and light intensity employed [12]. As observed, the mineralization levels measured by TOC and COD presented fair comparability. Moreover, the mineralization rate appears to be slower than the plastics degradation, owing to the accumulation of leached intermediates. In this regard, the nature of these oxidation by-products was evaluated through pyrolysis–gas chromatography/mass spectrometry (Pyr-GC–MS) and ion chromatography (IC). As the oxidation progressed, polycyclic (biphenyl, stilbene, chalcone, and naphthalene) and monocyclic aromatic hydrocarbons (benzaldehyde, acetophenone, and benzoic acid) were identified, along with short chain acids such as acetic, formic, malonic and oxalic acids [27]. Additionally, for low degradation levels, such as those reached in the first 30 min of the photo-oxidative treatment, similar conversion levels calculated from turbidity, TOC and COD were achieved. This is due to the fact that initial degradation rate is limited by the refractory nature of the starting polymer and/or the higher turbidity of the reaction medium. All in all, turbidity, TOC and COD measurements clearly provide representative conversion values for monitoring the progress of the advanced oxidation of NPs in water.

Fig. 10 shows the evolution in particle size of PS NPs (140 nm) upon photo-Fenton treatment (see the TEM analyses for larger particles in Figs. S2, S3 and S4 of the Supporting Information). As photo-oxidation proceeds, new surface functionalities begin to appear on PS NPs due to the breakdown of polymeric chains by the radicals attack, promoting particle agglomeration through surface adhesion and chain crosslinking [12,43]. Simultaneously, the individual particle size decreases, in accordance with turbidity measurements (Fig. 8a). For instance, after 60 min reaction time, PS NPs achieved a mean diameter of 56.9 nm and a volume reduction of 92.9 % (Table 2). Beyond 60 min, no particles were detected in the reaction medium. See Tables S1, S2 and S3 for particle size analysis of larger PS NPs. Again, the results from DLS indicated a larger mean diameter compared to those obtained by TEM (Table 2), likely due to the broader particle size distribution in oxidized samples and/or the formation of particle agglomerates. Moreover, AFM measurements demonstrated a good agreement with TEM analysis (Table 2 and Fig. S1), confirming the suitability of the technique for monitoring particle size.

These results are consistent with our previous studies on the degradation of PS NPs by Fenton and photo-Fenton oxidation, suggesting that the oxidative degradation starts on the NPs surface and proceeds toward the core while retaining their sphericity and increasing the particle size distribution [12,20]. Furthermore, as showed in Fig. 9c, the conversion of PS NPs calculated from TEM analysis align closely with the results

obtained from turbidity measurements. However, it should be noted that TEM analysis can underestimate the conversion of NPs, especially at advanced stages of the oxidation, due to the preferential counting of larger particles.

Typically, FTIR analysis of MPs/NPs involves the determination of the carbonyl index (CI) [13,31,44], enabling the monitoring of oxygen incorporation into the polymeric samples [20,25]. Ketones, aldehydes, carboxylic acids, and esters contain the carbonyl group ($C=O$) and absorb IR radiation in the wavenumber region 1870 – 1540 cm^{-1} . The constant position, high intensity, and minimal interference bands at that region make the carbonyl absorption band an excellent candidate to monitor the photodegradation progress [45]. In Fig. 11 and Fig. S5, the FTIR spectra of the oxidized PS NPs are displayed. Accordingly, Table 3 presents the CI values for both fresh and oxidized samples under study, demonstrating a significant increase in the CI as the photo-oxidation progresses. To a lesser extent, there was an absorption increase in the 1300 – 1000 cm^{-1} wavenumber region, which may be attributed to the stretching of $C-O$ single bonds [46]. These results clearly suggest the incorporation of oxygen atoms upon photo-Fenton treatment.

Additionally, the organic and inorganic constituents present in real water matrices can influence the oxidation yield, having neutral, inhibitory, or promoting effects [47]. To simulate a more realistic scenario, a secondary wastewater treatment plant effluent was spiked with PS NPs, and a new photo-Fenton test was conducted under the previously described conditions. As depicted in Fig. 12, the removal rate of PS NPs was delayed by 15 min for the test performed with a more realistic water matrix, but reached complete conversion in 105 min. Firstly, the $HO\bullet$ radicals are used to oxidize the dissolved organic matter present in the real wastewater, and then proceeds to the oxidation of the more refractory PS NPs, until complete disappearance. This result demonstrates the versatility of the photo-Fenton treatment.

Based on these findings, the photo-assisted degradation of PS NPs was thoroughly characterized using several analytical methods to monitor changes in concentration, mineralization, particle size, and chemical modifications. However, when dealing with realistic samples, it is expected the presence of additional sources of organic matter, higher degree of polydispersity and lower concentrations of NPs. To accurately characterize NPs, the organic-rich compounds must be removed first without altering NPs properties. Fenton's reagent could be a good alternative for the recovery of more realistic samples [48]. In cases of very low concentrations, sample preconcentration will be necessary. Moreover, the polydispersity of the sample should not significantly impact the measurements when utilizing bulk analyses such as turbidity, TOC, COD, or FTIR, or when conducting microscopy characterizations to representative particle populations.

4. Conclusions

The advanced oxidation of polystyrene nanoplastics (PS NPs) upon photo-Fenton treatment was thoroughly characterized using a combination of analytical techniques to monitor the evolution of concentration, mineralization, particle size, and chemical modifications of both fresh and oxidized nanoplastics in water. From these results, the following conclusions can be drawn:

- Turbidity measurements offer a fast and accurate method for determining the concentration of nanoplastics suspensions in water and their degree of degradation.
- The mineralization level of treated samples can be effectively determined by TOC and COD measurements. It is important to note that samples containing nanoplastics may cause permanent damage to the TOC instrument. Therefore, this analysis is recommended at advanced stages of the oxidative treatment or for monitoring small nanoparticles of c.a. 100 nm. Conversely, COD measurements allow for the complete digestion of non-soluble

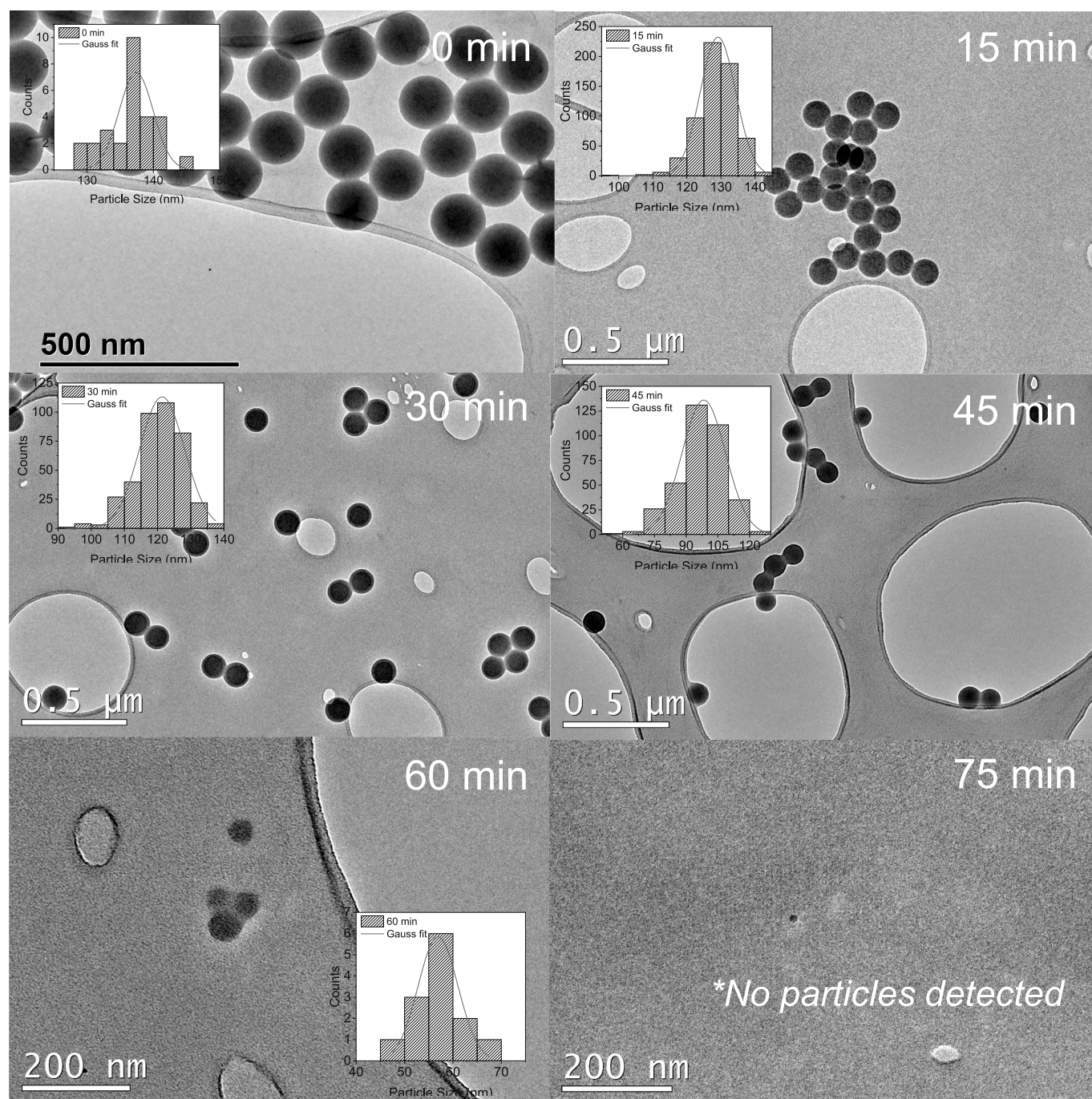


Fig. 10. TEM analysis for the photo-Fenton oxidation of PS NPs ($D_0 = 140$ nm; $[\text{PS NPs}]_0 = 100$ mg/L; $[\text{Fe}^{3+}]_0 = 1$ mg/L; $[\text{H}_2\text{O}_2]_0 = 1000$ mg/L (H_2O_2 dosed every 30 min, 500 mg/L); $\text{pH}_0 = 3$; $T = 25$ °C).

nanoplastics regardless of their size, providing reliable values of the oxidizable matter content.

- iii) Morphology and particle size can be accurately determined by TEM and AFM, while DLS and NTA did not perform well in characterizing these samples due to the formation of particle agglomerates and/or broader particle size distributions. Additionally, the degradation level can be calculated from particle size analysis, considering the particle geometry.
- iv) Chemical surface modifications, such as the incorporation of oxygenated groups, can be assessed by FTIR by calculating the carbonyl index. This parameter serves as a metric for the oxidation of polymers that do not have characteristic IR absorption

peaks in the wavenumber region of the carbonyl peak absorbance band.

CRediT authorship contribution statement

Carla di Luca: Writing – review & editing, Writing – original draft, Visualization, Validation, Methodology, Investigation, Formal analysis, Data curation, Conceptualization. **Jorge Garcia:** Validation, Methodology, Investigation, Data curation. **Macarena Munoz:** Writing – review & editing, Supervision, Resources, Project administration, Funding acquisition, Conceptualization. **Mercedes Hernando-Pérez:** Writing – review & editing, Methodology, Investigation. **Zahara M. de Pedro:** Writing – review & editing, Supervision, Resources, Project

Table 2

Evolution of mean particle diameter upon photo-Fenton oxidation of PS NPs ($D_0 = 140$ nm; $[PS\ NPs]_0 = 100$ mg/L; $[Fe^{3+}]_0 = 1$ mg/L; $[H_2O_2]_0 = 1000$ mg/L (H_2O_2 dosed every 30 min, 500 mg/L); $pH_0 = 3$; $T = 25$ °C).

Time (min)	Mean particle diameter (nm)			Volume reduction* (%)
	TEM	AFM	DLS	
0	137.4	137.7	149.7	0
15	124.1			26.3
30	121.3	117.3		31.1
45	98.3	96.8	132.3	63.4
60	56.9			92.9
75	Non detected			—
90	Non detected			—

*Calculated considering the radius reduction of spheres with the mean diameter determined from the Gaussian-like distribution of particle size in TEM images.

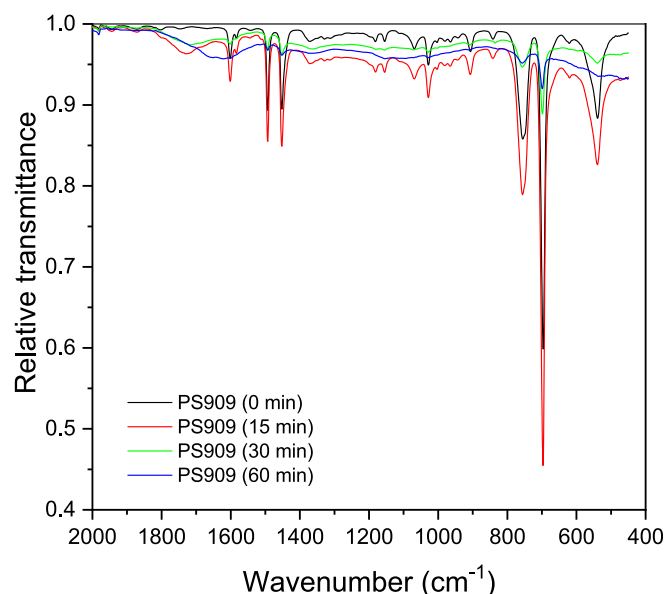


Fig. 11. FTIR spectra of fresh and oxidized PS NPs ($D_0 = 909$ nm; $[PS\ NPs]_0 = 100$ mg/L; $[Fe^{3+}]_0 = 1$ mg/L; $[H_2O_2]_0 = 1000$ mg/L (H_2O_2 dosed every 30 min, 500 mg/L); $pH_0 = 3$; $T = 25$ °C and $t = 30$ min).

Table 3

Carbonyl index of fresh and oxidized PS NPs. Oxidation conditions: $D_0 = 140$, 252, 460 and 909 nm; $[PS\ NPs]_0 = 100$ mg/L; $[Fe^{3+}]_0 = 1$ mg/L; $[H_2O_2]_0 = 1000$ mg/L (H_2O_2 dosed every 30 min, 500 mg/L); $pH_0 = 3$; $T = 25$ °C and $t = 30$ min.

Nominal diameter (nm)	Reaction time (min)	CI
140	0	0.208
140	30	1.95
252	0	0.217
252	30	2.68
460	0	0.142
460	30	2.18
909	0	0.115
909	15	0.961
909	30	2.15
909	60	1.93

administration, Funding acquisition, Conceptualization. **Jose A. Casas:** Writing – review & editing, Supervision, Resources, Project administration, Funding acquisition, Conceptualization.

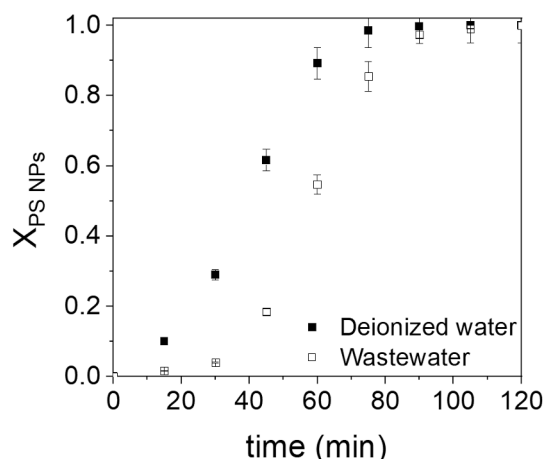


Fig. 12. Photo-Fenton oxidation of PS NPs: Effect of the water matrix ($D_0 = 140$ nm; $[PS\ NPs]_0 = 100$ mg/L; $[Fe^{3+}]_0 = 1$ mg/L; $[H_2O_2]_0 = 1000$ mg/L (H_2O_2 dosed every 30 min, 500 mg/L); $pH_0 = 3$; $T = 25$ °C).

Declaration of competing interest

The authors declare that they have no known competing financial interests or personal relationships that could have appeared to influence the work reported in this paper.

Data availability

Data will be made available on request.

Acknowledgments

This research has received support from the Spanish Ministry of Science and Innovation (MCIN) and AEI through the grant TED2021-131380B-C21 funded by MCIN/AEI/10.13039/501100011033 and European Union NextGenerationEU/PRTR, and through the grants PID2019-105079RB-I00 and PID2022-139063OB-I00 funded by MCIN/AEI/10.13039/501100011033 and by ERDF A way of making Europe. C. di Luca acknowledges financial support from the European Union's Horizon Europe research and innovation program under the Marie Skłodowska-Curie postdoctoral grant agreement N°: 101062665. M. Hernando-Pérez holds a Ramón y Cajal position (RyC2021-030929-I) funded by MCIN/AEI/10.13039/501100011033 and European Union NextGenerationEU/PRTR, Spain. She also acknowledges funding from 'Ayudas a Proyectos de I+D para Jóvenes Doctores de la Universidad Autónoma de Madrid 2021', SI3/PJI/2021-00216 supported by the Community of Madrid and UAM, and the grant TED2021-129937B-I00 funded by MCIN/AEI/10.13039/501100011033 and European Union NextGenerationEU/PRTR. The authors would like to express their gratitude to Dr. Marco Dondero for his technical support in programming and calculations related to the response surface. The authors acknowledge the characterization performed by NTA at the ICTS "NANBIOSIS", Unit 6, CIBER-BBN at the Barcelona Materials Science Institute, Spain.

Appendix A. Supplementary data

Supplementary data to this article can be found online at <https://doi.org/10.1016/j.cej.2024.152490>.

References

- [1] Plastics Europe, Plastics – the fast Facts 2023 (2023). Available in: <https://plasticseurope.org/knowledge-hub/plastics-the-fast-facts-2023/>.

- [2] D.E. MacArthur, D. Waughray, R.M. Stuchtey, The New Plastics Economy: Rethinking the Future of Plastics. World Economic Forum (2016). Available in: http://www3.weforum.org/docs/WEF_The_New_Plastics_Economy.pdf.
- [3] M. Enfrin, L.F. Dumée, J. Lee, Nano/microplastics in water and wastewater treatment processes – Origin, impact and potential solutions, *Water Res.* 161 (2019) 621–638, <https://doi.org/10.1016/j.watres.2019.06.049>.
- [4] Z. Chen, X. Shi, J. Zhang, L. Wu, W. Wei, B.-J. Ni, Nanoplastics are significantly different from microplastics in urban waters, *Water Research X* 19 (2023) 100169, <https://doi.org/10.1016/j.wroa.2023.100169>.
- [5] R. Lehner, C. Weder, A. Petri-Fink, B. Rothen-Rutishauser, Emergence of Nanoplastic in the Environment and Possible Impact on Human Health, *Environ. Sci. Technol.* 53 (2019) 1748–1765, <https://doi.org/10.1021/acs.est.8b05512>.
- [6] I. Ali, T. Ding, C. Peng, I. Naz, H. Sun, J. Li, J. Liu, Micro- and nanoplastics in wastewater treatment plants: Occurrence, removal, fate, impacts and remediation technologies – A critical review, *Chem. Eng. J.* 423 (2021) 130205, <https://doi.org/10.1016/j.cej.2021.130205>.
- [7] J. Sun, X. Dai, Q. Wang, M.C.M. Van Loosdrecht, B.-J. Ni, Microplastics in wastewater treatment plants: Detection, occurrence and removal, *Water Res.* 152 (2019) 21–37, <https://doi.org/10.1016/j.watres.2018.12.050>.
- [8] Y. Jeong, G. Gong, H.-J. Lee, J. Seong, S.W. Hong, C. Lee, Transformation of microplastics by oxidative water and wastewater treatment processes: A critical review, *J. Hazard. Mater.* 443 (2023) 130313, <https://doi.org/10.1016/j.jhazmat.2022.130313>.
- [9] O.M. Rodríguez-Narvaez, A. Goonetilleke, L. Perez, E.R. Bandala, Engineered technologies for the separation and degradation of microplastics in water: A review, *Chem. Eng. J.* 414 (2021) 128692, <https://doi.org/10.1016/j.cej.2021.128692>.
- [10] M. Shen, B. Song, C. Zhou, T. Hu, G. Zeng, Y. Zhang, Advanced oxidation processes for the elimination of microplastics from aqueous systems: Assessment of efficiency, perspectives and limitations, *Sci. Total Environ.* 842 (2022) 156723, <https://doi.org/10.1016/j.scitotenv.2022.156723>.
- [11] Z. Chen, X. Liu, W. Wei, H. Chen, B.-J. Ni, Removal of microplastics and nanoplastics from urban waters: Separation and degradation, *Water Res.* 221 (2022) 118820, <https://doi.org/10.1016/j.watres.2022.118820>.
- [12] C. di Luca, J. Garcia, D. Ortiz, M. Munoz, J. Carbajo, Z.M. De Pedro, J.A. Casas, Mineralization of polystyrene nanoplastics in water by photo-Fenton oxidation, *J. Environ. Chem. Eng.* 11 (2023) 110755, <https://doi.org/10.1016/j.jece.2023.110755>.
- [13] M.R. Karimi Estahbanati, M. Kiendrebego, A. Khosravanipour Mostafazadeh, P. Drogui, R.D. Tyagi, Treatment processes for microplastics and nanoplastics in waters: State-of-the-art review, *Marine Pollution Bulletin* 168 (2021) 112374, <https://doi.org/10.1016/j.marpolbul.2021.112374>.
- [14] N.D.O. Dos Santos, R. Busquets, L.C. Campos, Insights into the removal of microplastics and microfibrils by Advanced Oxidation Processes, *Sci. Total Environ.* 861 (2023) 160665, <https://doi.org/10.1016/j.scitotenv.2022.160665>.
- [15] L.P. Domínguez-Jaimes, E.I. Cedillo-González, E. Luévano-Hipólito, J.D. Acuña-Bedoya, J.M. Hernández-López, Degradation of primary nanoplastics by photocatalysis using different anodized TiO₂ structures, *J. Hazard. Mater.* 413 (2021) 125452, <https://doi.org/10.1016/j.jhazmat.2021.125452>.
- [16] T. Easton, V. Koutsos, E. Chatzisympson, Removal of polyester fibre microplastics from wastewater using a UV/H₂O₂ oxidation process, *J. Environ. Chem. Eng.* 11 (2023) 109057, <https://doi.org/10.1016/j.jece.2022.109057>.
- [17] Y. Cai, F. Chen, L. Yang, L. Deng, Z. Shi, Degradation of Polystyrene Nanoplastics in UV/NaClO and UV/PMS Systems: Insights into Degradation Efficiency, Mechanism, and Toxicity Evaluation, *Water* 15 (2023) 1920, <https://doi.org/10.3390/w15101920>.
- [18] Y. Li, J. Li, J. Ding, Z. Song, B. Yang, C. Zhang, B. Guan, Degradation of nano-sized polystyrene plastics by ozonation or chlorination in drinking water disinfection processes, *Chem. Eng. J.* 427 (2022) 131690, <https://doi.org/10.1016/j.cej.2021.131690>.
- [19] Y. Li, C. Zhang, C. Shen, G. Jiang, B. Guan, Enhanced ozonation of polystyrene nanoplastics in water with CeO_x/MnO_x catalyst, *Environ. Res.* 220 (2023) 115220, <https://doi.org/10.1016/j.envres.2023.115220>.
- [20] D. Ortiz, M. Munoz, J. Nieto-Sandoval, C. Romera-Castillo, Z.M. de Pedro, J. A. Casas, Insights into the degradation of microplastics by Fenton oxidation: From surface modification to mineralization, *Chemosphere* 309 (2022) 136809, <https://doi.org/10.1016/j.chemosphere.2022.136809>.
- [21] K. Tanaka, Y. Takahashi, H. Kuramochi, M. Osako, S. Tanaka, G. Suzuki, Preparation of Nanoscale Particles of Five Major Polymers as Potential Standards for the Study of Nanoplastics, *Small* 17 (2021) 2105781, <https://doi.org/10.1002/smll.202105781>.
- [22] F. Blanco, M. Davranche, H.E. Hadri, B. Grassl, J. Gigault, Nanoplastics Identification in Complex Environmental Matrices: Strategies for Polystyrene and Polypropylene, *Environ. Sci. Technol.* 55 (2021) 8753–8759, <https://doi.org/10.1021/acs.est.1c01351>.
- [23] J.D. Acuña-Bedoya, E. Luévano-Hipólito, E.I. Cedillo-González, L.P. Domínguez-Jaimes, A.M. Hurtado, J.M. Hernández-López, Boosting visible-light photocatalytic degradation of polystyrene nanoplastics with immobilized CuO obtained by anodization, *J. Environ. Chem. Eng.* 9 (2021) 106208, <https://doi.org/10.1016/j.jece.2021.106208>.
- [24] P.H. Allé, P. Garcia-Muñoz, K. Adouby, N. Keller, D. Robert, Efficient photocatalytic mineralization of polymethylmethacrylate and polystyrene nanoplastics by TiO₂/β-SiC alveolar foams, *Environ Chem Lett* 19 (2021) 1803–1808, <https://doi.org/10.1007/s10311-020-01099-2>.
- [25] K. Hu, P. Zhou, Y. Yang, T. Hall, G. Nie, Y. Yao, X. Duan, S. Wang, Degradation of Microplastics by a Thermal Fenton Reaction, *ACS EST Eng.* 2 (2022) 110–120, <https://doi.org/10.1021/acsestengg.1c00323>.
- [26] V. Piazza, A. Uheida, C. Gambardella, F. Garaventa, M. Faimali, J. Dutta, Ecosafety Screening of Photo-Fenton Process for the Degradation of Microplastics in Water, *Front. Mar. Sci.* 8 (2022) 791431, <https://doi.org/10.3389/fmars.2021.791431>.
- [27] Z. Martínez de Pedro, J. García, C. di Luca, A. Abarkan, L. Cherta, M. Munoz, J.A. Casas, “Removal of polystyrene nanoplastics via optimized photo-Fenton process: structural analysis and degradation pathways”. *Proc. of VI Iberoamerican Conference on Advanced Oxidation Technologies (VI CIPOA)*, Florianópolis, Brazil, 2024.
- [28] S. Clesceri, A.E. Greenberg, A.D. Eaton, *Standard Methods for the Examination of Water and Wastewater*, 20th ed., American Public Health Association, 1998.
- [29] D.W. O’Sullivan, M. Tyree, The kinetics of complex formation between Ti(IV) and hydrogen peroxide, *Int J of Chemical Kinetics* 39 (2007) 457–461, <https://doi.org/10.1002/kin.20259>.
- [30] I. Horcas, R. Fernández, J.M. Gómez-Rodríguez, J. Colchero, J. Gómez-Herrero, A. M. Baro, WSXM : A software for scanning probe microscopy and a tool for nanotechnology, *Rev. Sci. Instrum.* 78 (2007) 013705, <https://doi.org/10.1063/1.2432410>.
- [31] P. García-Muñoz, P.H. Allé, C. Bertoloni, A. Torres, M.U. De La Orden, J. M. Urreaga, M.-A. Dziurla, F. Fresno, D. Robert, N. Keller, Photocatalytic degradation of polystyrene nanoplastics in water. A methodological study, *Journal of Environmental Chemical Engineering* 10 (2022) 108195, <https://doi.org/10.1016/j.jece.2022.108195>.
- [32] A. Bianco, F. Sordello, M. Ehn, D. Vione, M. Passananti, Degradation of nanoplastics in the environment: Reactivity and impact on atmospheric and surface waters, *Sci. Total Environ.* 742 (2020) 140413, <https://doi.org/10.1016/j.scitotenv.2020.140413>.
- [33] L. Tian, Q. Chen, W. Jiang, L. Wang, H. Xie, N. Kalogerakis, Y. Ma, R. Ji, A carbon-14 radiotracer-based study on the phototransformation of polystyrene nanoplastics in water versus in air, *Environ. Sci. Nano* 6 (2019) 2907–2917, <https://doi.org/10.1039/C9EN00662A>.
- [34] J.-M. Lee, R. Busquets, I.-C. Choi, S.-H. Lee, J.-K. Kim, L.C. Campos, Photocatalytic Degradation of Polyamide 66; Evaluating the Feasibility of Photocatalysis as a Microfibre-Targeting Technology, *Water* 12 (2020) 3551, <https://doi.org/10.3390/w12123551>.
- [35] S. Mariano, S. Tacconi, M. Fidaleo, M. Rossi, L. Dini, Micro and Nanoplastics Identification: Classic Methods and Innovative Detection Techniques, *Front. Toxicol.* 3 (2021) 636640, <https://doi.org/10.3389/ftox.2021.636640>.
- [36] W. Fu, J. Min, W. Jiang, Y. Li, W. Zhang, Separation, characterization and identification of microplastics and nanoplastics in the environment, *Sci. Total Environ.* 721 (2020) 137561, <https://doi.org/10.1016/j.scitotenv.2020.137561>.
- [37] P. Rademeyer, D. Carugo, J.Y. Lee, E. Stride, Microfluidic system for high throughput characterisation of ecogenic particles, *Lab Chip* 15 (2015) 417–428, <https://doi.org/10.1039/C4LC001206B>.
- [38] F. Caputo, R. Vogel, J. Savage, G. Vella, A. Law, G. Della Camera, G. Hannon, B. Peacock, D. Mehn, J. Ponti, O. Geiss, D. Aubert, A. Prina-Mello, L. Calzolari, Measuring particle size distribution and mass concentration of nanoplastics and microplastics: addressing some analytical challenges in the sub-micron size range, *J. Colloid Interface Sci.* 588 (2021) 401–417, <https://doi.org/10.1016/j.jcis.2020.12.039>.
- [39] G. Binnig, C.F. Quate, Ch. Gerber, Atomic Force Microscope, *Phys. Rev. Lett.* 56 (1986) 930–933, <https://doi.org/10.1103/PhysRevLett.56.930>.
- [40] S. Adhikari, V. Kelkar, R. Kumar, R.U. Halden, Methods and challenges in the detection of microplastics and nanoplastics: a mini-review, *Polym. Int.* 71 (2022) 543–551, <https://doi.org/10.1002/pi.6348>.
- [41] C.F. Araújo, M.M. Nolasco, A.M.P. Ribeiro, P.J.A. Ribeiro-Claro, Identification of microplastics using Raman spectroscopy: Latest developments and future prospects, *Water Res.* 142 (2018) 426–440, <https://doi.org/10.1016/j.watres.2018.05.060>.
- [42] B.C. Smith, The Infrared Spectra of Polymers III: Hydrocarbon Polymers, *Spectroscopy* (2021) 22–25, <https://doi.org/10.56530/spectroscopy.mh7872q7>.
- [43] E. Yousif, R. Haddad, Photodegradation and photostabilization of polymers, especially polystyrene: review, *Springerplus* 2 (2013) 398, <https://doi.org/10.1186/2193-1801-2-398>.
- [44] T.S. Tofa, K.L. Kunjali, S. Paul, J. Dutta, Visible light photocatalytic degradation of microplastic residues with zinc oxide nanorods, *Environ Chem Lett* 17 (2019) 1341–1346, <https://doi.org/10.1007/s10311-019-00859-z>.
- [45] V. Mylläri, T. Ruoko, S. Syrjälä, A comparison of rheology and FTIR in the study of polypropylene and polystyrene photodegradation, *J of Applied Polymer Sci* 132 (2015) app.42246, <https://doi.org/10.1002/app.42246>.
- [46] B.C. Smith, The C-O Bond, Part I: Introduction and the Infrared Spectroscopy of Alcohols, *Spectroscopy* (2017) 6–11, <https://doi.org/10.56530/spectroscopy.vz517012>.
- [47] A.R. Lado Ribeiro, N.F.F. Moreira, G. Li Puma, A.M.T. Silva, Impact of water matrix on the removal of micropollutants by advanced oxidation technologies, *Chem. Eng. J.* 363 (2019) 155–173, <https://doi.org/10.1016/j.cej.2019.01.080>.
- [48] R.R. Hurley, A.L. Lusher, M. Olsen, L. Nizzetto, Validation of a Method for Extracting Microplastics from Complex, Organic-Rich, Environmental Matrices, *Environ. Sci. Technol.* 52 (2018) 7409–7417, <https://doi.org/10.1021/acs.est.8b01517>.